Design guidelines for supersonic radial vanes operating with non-ideal flow conditions.

Nitish Anand[1*], Piero Colonna[2], Matteo Pini[3]

[1,2,3] Propulsion and Power, TU Delft,
Delft, Netherlands
n.anand@tudelft.nl[1*]
* Corresponding Author

ABSTRACT

Supersonic stator vanes of high temperature mini-Organic Rankine Cycle (ORC) turbines account for two-thirds of the fluid-dynamic losses. As a result, the overall performance of the turbo-expander primarily depends on the design of stator vanes. Currently, there is no established correlation for the optimal design of ORC stators. In this work, the accuracy of the only design law applicable to ORC stators, the Deich's model, is investigated. A physics-based analytical model and a CFD-based numerical model were developed to obtain the optimal post-expansion ratio and to compare their results with the Deich's model. The analysis shows that the Deich's method fails to accurately predict the optimum value of the post-expansion ratio. In summary, vanes operating with a complex fluid and given pressure ratio feature a unique value of the optimum post-expansion ratio and new correlations are required to predict its value. Future work will focus on the development of such correlations.

1. INTRODUCTION

High-expansion ratio is a defining feature of many turbo machines in the recent past, which, therefore often operate at supersonic flow conditions. As a result, this trend catalyzes the development of new turbomachinery design methods. ORC turbines are characterized by high-expansion ratio and are often supersonic (White and Sayma, 2016). ORC power systems are becoming increasingly relevant because they can convert thermal energy from renewable and waste heat sources (Colonna et al., 2015). Regardless of its wide application, the full potential of ORC technology is not realized yet. Economic viability will increase if current technical challenges are overcome. One issue affecting turbine design and performance is the complex and non-ideal fluid dynamics in the stator. A previous study by Rinaldi et al. (2016) highlights that the stator vanes of an ORC turbine account for approximately two-thirds of the fluid-dynamic losses of the turbine, especially if the stage is highly loaded. Therefore, the design of stator blades is critical.

The preliminary design phase of these vanes involves the choice of parameters, e.g., solidity, degree of divergence (DoD), etc., based on correlations. The blade profile is then obtained with the Method of Characteristics (MoC) and refined by means of CFD simulation. The mechanical verification completes the design iteration. The recent studies on vanes by Anand et al. (2018) and Guardone et al. (2013) focus on the detailed fluid dynamic design of ORC stators. However, there is no study in the literature on the choice of preliminary design parameters which dictate the detailed design phase. Currently, therefore, correlations that were developed for gas turbines are used, and the optimal design of such blades can be only obtained by resorting to expensive numerical optimization based on high-fidelity CFD.

To the authors' knowledge, the only existing model that can be employed to define the degree of divergence, i.e., the ratio between the nozzle outlet section and the nozzle throat section, at preliminary design level, is the one proposed by Deich et al. (1965). This model provides the optimum degree of nozzle divergence as a function of stator exit Mach number. Additionally, the model was exclusively derived for supersonic axial cascades operating with perfect gases, therefore its application to the design of supersonic vanes operating with non-ideal compressible flows is debatable. The objective of this paper is

to discuss the accuracy and limitations of the Deich's model, henceforth referred to as *empirical* method, if applied to nozzles affected by non-ideal compressible fluid dynamic effects.

To achieve this goal, a physics-based and a CFD-based loss estimation model, restricted for now to perfect gas flows, were developed and these are referred to as *analytical* and *CFD-based* methods in the following.

The analytical method estimates the boundary-layer and mixing losses for a typical supersonic axial vane configuration. The losses in the boundary-layer are evaluated by following Denton (1993). The mixing loss is evaluated by means of the flow deviation angle, which is determined by applying mass, momentum and energy conservation at the semi-bladed region of the stator vane (Osnaghi, 2013).

The CFD-based method comprises of a detail design procedure and of a CFD simulation. The vane geometry generation method is adapted to handle axial configurations from the method described byAnand et al. (2018). The fluid-dynamic performance of the blades is calculated using the open-source Reynolds averaged Navier Stokes (RANS) solver SU2 and the flow equations are complemented by the one-equation Spalart-Allmaras turbulence model.

To investigate the accuracy of the empirical model, the optimum DoD (or alternatively, the optimum post-expansion ratio) obtained from this model is compared to those resulting from the numerical and the analytical methods. Additionally, the analysis is extended to fluids ranging from simple fluids, like air, to complex fluids, like MM, to study the effect of molecular complexity on the optimum post-expansion ratio.

2. METHODOLOGY

The flow domain of a typical axial stator vane can be divided into three sections, namely, see Figure 1(a), the converging section between station (t) and (o), the diverging section between station (o) and (a) and the semi-bladed section between station (a) and (1). To compare the optimum DoD from the empirical method, losses in vanes with varying DoD is estimated using analytical and CFD-based method.

2.1 Empirical Method

Deich in 1965 suggested one of the only methods to define the DoD for a stator vane operating with transonic/supersonic flow conditions. According to this method, the DoD is provided by the relation

$$\mathrm{DoD}_{\mathrm{empirical}} = \frac{A_\mathrm{a}}{A_\mathrm{o}} = \begin{cases} 1, & \text{for } M_1 \le 1.4, \\ 1 + (0.5\,M_1 - 0.4)\left[\dfrac{1}{A_\mathrm{is}(M_1,\gamma)} - 1\right], & \text{for } M_1 > 1.4, \end{cases} \tag{1}$$

where M_1 is the stator design Mach number, A_o is nozzle throat width, A_a is nozzle outlet width, A_is is the area ratio corresponding to an isentropic expansion and γ is the heat capacity ratio. The underlying hypothesis is that nozzles with M_1 lower than 1.4 (transonic) do not require the diverging section, because the semi-bladed section is sufficient. For M_1 greater than 1.4 (supersonic) a diverging section is necessary.

2.2 Analytical Method

Two of the major dissipation mechanisms in supersonic axial vanes are mixing and boundary layer losses. The procedure to analytically estimate these losses is as follows:

(a) Mixing losses are estimated with the flow deviation angle relation ($\Delta\phi$) proposed by Osnaghi (2013). The equation is derived by solving the mass, momentum and energy conservation equations in the control

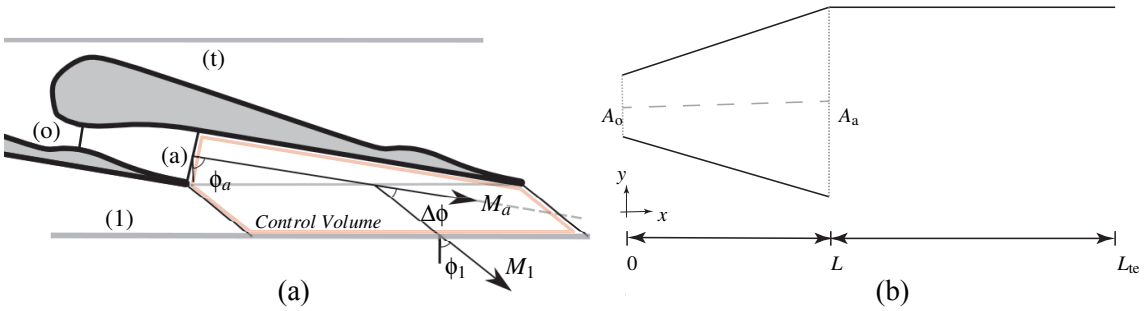

Figure 1: Schematics of the geometry for the analytical loss models: (a) geometry for the mixing loss model, showing different stations in the supersonic vane, Mach number and deviation angle. Control volume outlined in red. (b) geometry for the boundary layer loss model, showing the diverging and the linear suction side sections.

volume encompassing the semi-bladed section of the vane. The flow deviation angle is

$$\Delta\phi = \arctan\left[\frac{\frac{\gamma}{1-\gamma}\beta_{1a}\tan\phi_a \pm \sqrt{\left(1-\beta_{1a}\right)\left(2\frac{\gamma}{\gamma-1}M_a^2 - 1 - \frac{\gamma+2}{\gamma-1}\beta_{1a}\right) + \left(\frac{\gamma}{\gamma-1}\beta_{1a}\tan\phi_a\right)^2}}{1+\gamma M_a^2 - \beta_{1a}}\right], \tag{2}$$

where, M_a is the nozzle Mach number, ϕ_a is the design flow angle and $\beta_{1a}^{-1} \equiv \beta_{a1}$ is the post-expansion ratio. The only independent quantity in (2) is β_{1a} which allows to evaluate M_1 at the exit of the vane. Thus, the kinetic energy dissipated can be estimated as

$$\xi_{MIX} = \frac{H_1 - H_{is,1}}{H_{is,1}}, \tag{3}$$

where, H is enthalpy, and subscript "is" stands for isentropic.

(b) Boundary layer losses are due to viscous dissipation near the wall of the stator. Assuming turbulent flow on the blade surface, the kinetic energy dissipation is given

$$\xi_{BL} = \frac{\Delta H_{BL}}{H_{is,1}}, \tag{4}$$

where,

$$\Delta H_{BL} = T_1\dot{S} = T_1\frac{C_d\,\rho_T}{T_T}\int_0^X \frac{\rho_{xT}(M_x)}{T_{xT}(M_x)}M_x^3 c_x^3 dx \qquad \text{and} \tag{5}$$

$$H_{is,1} = 0.5\cdot\dot{m}v_{is,1}^2. \tag{6}$$

In these equations, C_d is the dissipation coefficient and is equal to 0.002 according to Denton (1993), ρ is the density, T is the temperature, S is the entropy, $\dot{m}$ is the mass flow rate, v is the velocity, c is the speed of sound and subscript "xT" stands for isentropic ratio.

The only unknown in equation (5) is the property distribution on the surface of the stator for which a quasi-1D flow model is assumed. Since the boundary layer losses in the subsonic section are significantly lower than the supersonic section (as boundary layer losses scale with the cube of the Mach number), only the diverging part of the nozzle and the semi-bladed section are modeled for simplicity. In the diverging section of the nozzle the flow accelerates, while in the semi-bladed section the linear suction side surface guides the flow to the outlet (see Figure 1). A quasi-1D model with linearly increasing area from A_o to A_a is assumed fro the nozzled, see Figure 1(b). Subsequently, the Mach number is assumed to

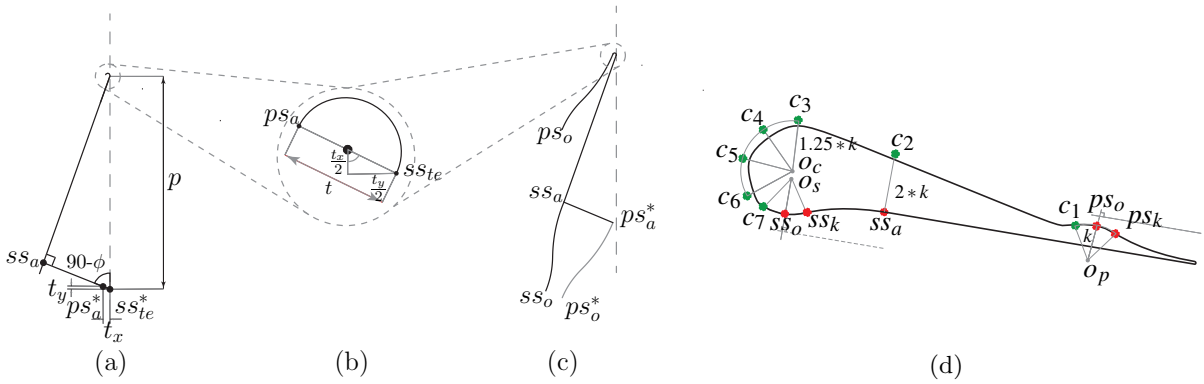

Figure 2: Steps to construct an axial supersonic vane, (a) semi-bladed region, (b) trailing edge (c) diverging-nozzle section and (d) converging section.

vary linearly from unity to the M_a. The suction side is modeled as a flat plate over which the fluid flows at constant Mach number M_a. Equation (5) allows to write the boundary layer loss in the vane as

$$\xi_{BL,ss} = 2\xi_{BL}|_0^L + \xi_{BL}|_L^{L_{te}}, \tag{7}$$

where, $\xi_{BL}|_0^L$ is the loss due one nozzle surface and $\xi_{BL}|_L^{L_{te}}$ is due the the loss on linear suction side. The optimum β_{a1} corresponds to the best performing vane from a set of vanes operating with varying DoD.

2.3 CFD-based Method

The vane geometries with varying DoD are generated and analyzed by following a procedure which can be divided into two parts, namely, Geometry Generation and CFD simulation. The procedure is similar to that documented by Anand et al. (2018) for radial vanes, however, it differs regarding the construction of the axial vane.

2.3.1 Geometry Generation. In order to design an axial supersonic stator, the nozzle geometry obtained by applying the MoC is adapted to the vane configuration and the converging section is constructed with Non-Uniform Rational Basis Splines (NURBs). Details of this MoC are illustrated by Anand et al. (2018), while the procedure to generate the vane geometry starting from the nozzle obtained with the MoC is as follows.

1. Scaling factor. With reference to Figure 2(a) and (b), two points ss_{te} and ss_{te}^*, which are a pitch-distance (p) apart, are placed on the plane where the trailing edge of the stator is to end. Next, point ss_a is defined by the intersection of the line originating from point ss_{te} at flow angle ϕ and the line originating from ss_{te}^* at an angle $90 - \phi$. This gives the line ss_a-ss_{te}, see Figure 2(a) and (d). Point ps_a^* is defined at a distance t (trailing edge thickness) from point ss_{te}^* along the line ss_{te}^*-ss_a. The diverging-nozzle geometry obtained with the MoC is scaled so as to have a throat width of unity, thus defining the exit area of the diverging-nozzle as $A_{is}(M_a)$. In order to complete the construction of the diverging part of the nozzle, the outlet cross-section area calculated with the MoC must be made the same as ss_a-ps_a^*. This is accomplished with a scaling factor determined by calculating the ratio of the distance between points ss_a-ps_a^* and $A_{is}(M_a)$. This can be mathematically written as

$$SF = \frac{l(ss_a, ps_a^*)}{A_{is}(M_a)}, \tag{8}$$

where, l is the length between ss_a and ps_a^*.

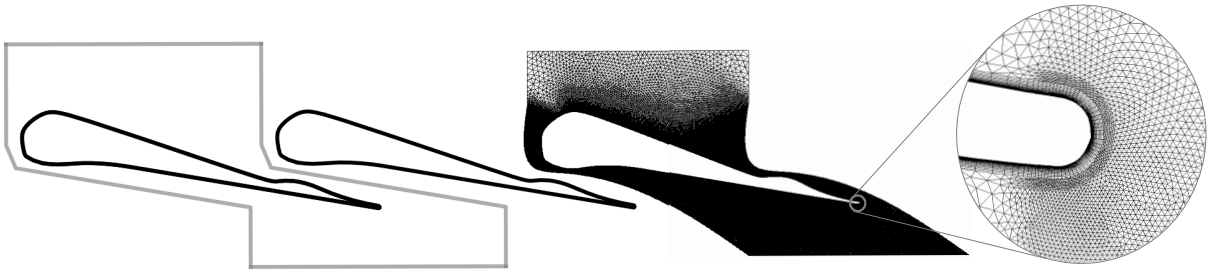

Figure 3: Vane geometry with computational flow domain outlined in gray (left) and discretized computational domain with zoomed-in view of the trailing edge (right).

2. Transformation of the nozzle geometry. The nozzle geometry obtained with the MoC is scaled to the factor (*SF*) obtained in step (1). The scaled nozzle is then rotated by angle ϕ about the center of the throat. The obtained nozzle constitutes the diverging section of the supersonic vane, see Figure 2(c).
3. Translation of the pressure side (line ps^*). To make the pressure and the suction side of the nozzle part of the same blade, the pressure side of the nozzle, section ps^* in Figure 2(c), is translated by a pitch-length to obtain curve *ps*.
4. Converging section. The converging section of the nozzle vane is constructed by means of a single NURBs curve connecting the throat points ss_o and ps_o through points c_1-c_7; see Figure 2(d).

2.3.2 CFD simulation. The performance of the supersonic vanes is computed using the open-source CFD software tool SU2 (Vitale et al., 2017). The computational domain encompassing one vane geometry is generated using UMG2, an in-house meshing tool (Ghidoni et al., 2006). An exemplary geometry is illustrated in Figure 3. The computational domain is discretized using clustered quadrilateral elements close to the wall, ensuring a $y^+ < 1$, and triangular elements in the rest of the domain. The flow equations are solved using the RANS model and the turbulence equations are closed using the one-equation Spalart-Allmaras model. The thermo-physical properties are calculated using the perfect gas model.

The flow domain is initialized by imposing a uniform state with properties equal to the total conditions at the inlet, and a back-pressure at the outlet. In addition, the non-reflective boundary condition, see Giles (1990), is also set. The solution was obtained by using an Euler Implicit time-marching scheme with a CFL of 10 while ensuring a second-order spatial accuracy. Residual reduction of 4 orders of magnitude was ensured by running the simulations for a maximum of 4000 iterations.

The kinetic energy loss coefficient, accounting for both boundary-layer and mixing losses, is calculated numerically by obtaining mixed-out average quantities at the boundaries, resulting in

$$\xi_{\mathrm{cfd}} = \frac{\bar{H}_1 - H_{\mathrm{is},1}}{0.5 \cdot v_{\mathrm{is},1}^2}, \tag{9}$$

where, $\bar{H}_1$ is the averaged enthalpy at the outlet of the stator domain.

3. TEST CASES

These methods are applied to a range of stator vanes operating at the same pressure ratio (β_{t1}) but with varying β_{a1} and fluid. β_{a1} of the vane is varied so as to capture the post-compression ($\beta_{a1} < 1$) and -expansion ($\beta_{a1} > 1$) phenomena in the semi-bladed section of the stator vane. The fluids under investigation range from fluids made of simple molecules to fluids made of complex molecules. This wide range enables to capture the variation of optimum β_{a1} ($\beta_{opt,a1}$) with respect to molecular complexity.

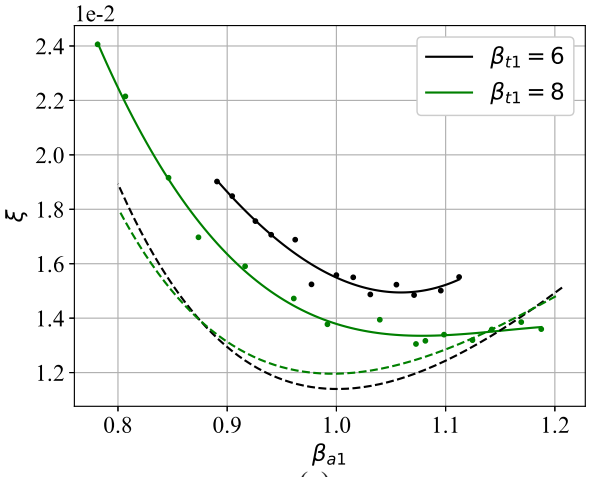

(a)

Method	$\beta_{opt,a1}$	
	$\beta_{t1} = 6$	$\beta_{t1} = 8$
Empirical	1.428	1.401
Analytical	1.0032	1.0036
CFD-based	1.059	1.078

(b)

Figure 4: Variation of $\beta_{opt,a1}$ with β_{t1} calculated with the analytical and the numerical methods. (a) trends showing the variation of ξ with β_{a1} for different β_{t1}, (b) $\beta_{opt,a1}$ obtained with the three methods.

The selected fluids are therefore Air, CO_2, Toluene and MM with γ of 1.4, 1.3, 1.055 and 1.025, respectively.

The stator vanes are designed for a ϕ_a of 70°. The solidity of the vane is constrained to unity in all the calculations implementing the methods selected for the comparison. The test vanes operate at a β_{t1} of 6.

4. RESULTS

The three methods, namely the empirical, the analytical and the CFD-based methods, are used to calculate the degree of divergence which ensures the least amount of fluid-dynamic losses for the above mentioned test cases.

As apparent from equation (1), the empirical method provides the value of optimum DoD, thus of $\beta_{opt,a1}$, according to the downstream Mach number M_1, which is in turn a function of β_{t1}. Figure 4 reports the $\beta_{opt,a1}$ obtained using the three methods for the stator vane operating with *MM* and for two values of the expansion ratio. The empirical method predicts a much higher $\beta_{opt,a1}$ as compared to the other two methods. This arguably means that the method underestimates the magnitude of the mixing losses, thus suggesting a reduction of the expansion ratio in the nozzle. Similar results are obtained for air. Further analysis would be needed to clearly identify the limitations of the method.

Figure 5(a) illustrates results calculated with the analytical method, that is, the trend of boundary-layer losses, mixing losses and total losses as a function of β_{a1}. As expected, the mixing losses are minimum at β_{a1} of unity and boundary-layer losses increase with nozzle exit Mach number, i.e., with decreasing β_{a1}. Moreover, the absolute values of boundary layer losses are found to be lower than that of mixing losses. Finally, both boundary-layer and mixing losses are higher for complex fluid molecules. The reason thereof is possibly related to the higher flow Mach number induced by the heavy fluid molecules for the same operating conditions of the vane.

The trend of total loss ξ_{tot} allows one to conclude that the different fluids in the flow cause varying $\beta_{opt,a1}$ values, which are however close to unity, as mixing-losses dominate the total loss in the stator.

The fluid-dynamic performance of the exemplary vanes are also calculated using the CFD-based method. The solidity is maintained within 1 ± 0.01 in accordance with the assumption made for the analytical

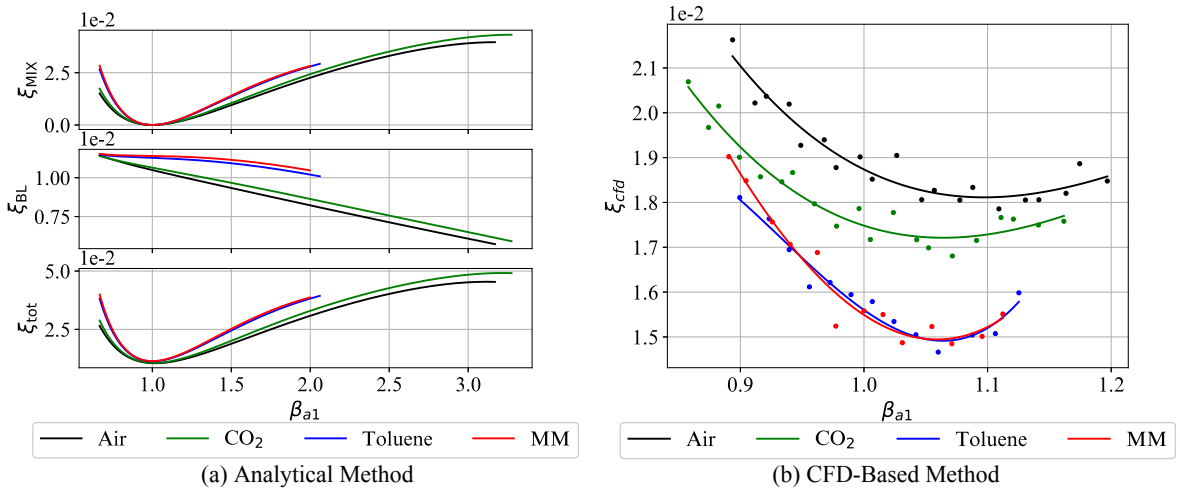

Figure 5: Optimum β_{a1} for different fluids operating at β_{t1} = 6.

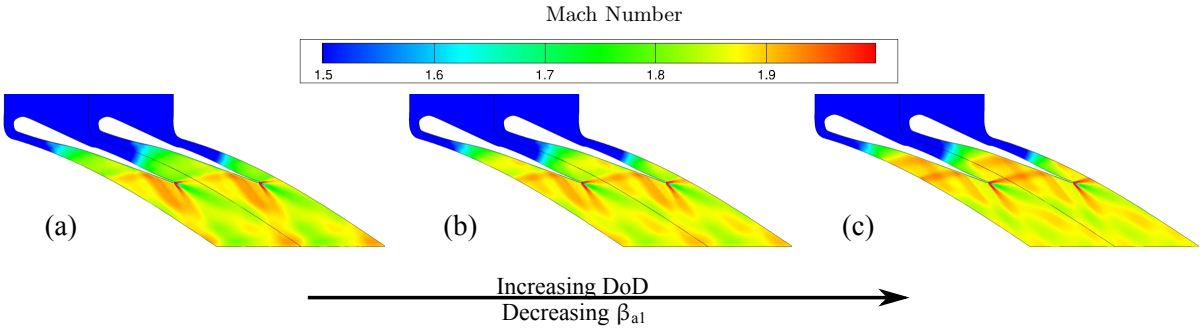

Figure 6: Mach number contours of vanes operating with Toluene at β_{t1} of 6 and with decreasing β_{a1} from left to right.

method. Figure 5(b) illustrates the variation of the vane performance with β_{a1}. The dots represent the numerically obtained values while the solid lines are a cubic fitting of the points. As opposed to the previous findings, it can be observed that the total loss is inversely proportional to the fluid molecular complexity, i.e., is higher in flows of simpler fluid molecules. This is attributed to shock-wave losses and the dissipation due to the impingement of the shock-wave on the suction side of the blade. Nonetheless, as found in the previous analysis, the mixing loss increases more significantly in flows made of complex fluid molecules, while departing from the optimal post-expansion ratio. Finally, it can be seen that there is a distinct $\beta_{opt,a1}$ value for each fluid which increases with decreasing molecular complexity.

Figure 6 depicts the Mach number contours for stator vanes operating with Toluene at β_{t1} of 6 with decreasing β_{a1} (or increasing DoD), with the Mach contour of Figure 6(b) being the one corresponding to the optimal post-expansion ratio. In all cases, a fishtail shock pattern originates at the trailing-edge of the vane. It can be seen that the strength of the pressure wave reflecting on the suction side increases with increasing DoD. This is because the flow exiting the nozzle in (c) undergoes a compression ($\beta_{a1} < 1$), while for case (a) and (b) the flow is further expanded ($\beta_{a1} > 1$). The mixing-out of the two pressure waves downstream eventually dictates the magnitude of the deflection angle and the associated mixing-loss.

The $\beta_{opt,a1}$ obtained from the three methods are plotted against γ in Figure 7(a). This figure also shows that the trends obtained with the three methods are similar and that flows of fluids made of complex molecules exhibit lower $\beta_{opt,a1}$. Moreover, the value of $\beta_{opt,a1}$ calculated using the empirical method is much higher than the value predicted by the other two methods for all the fluids.

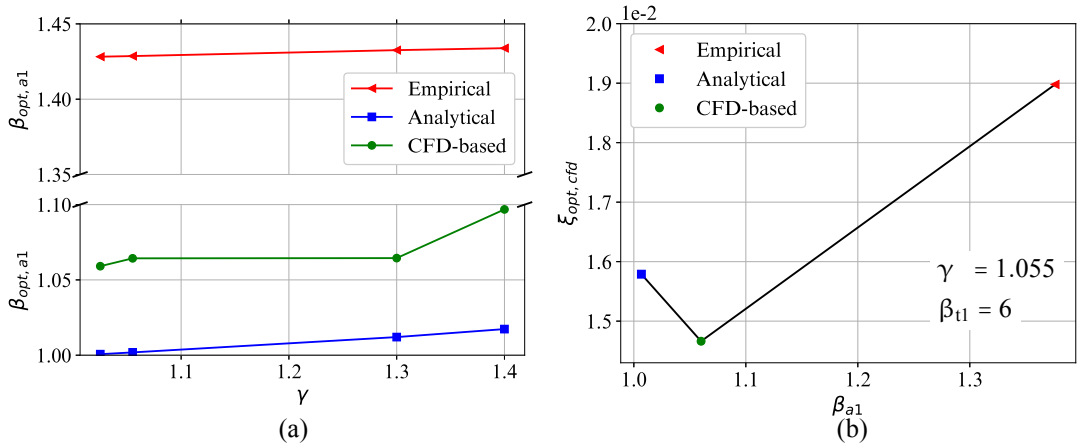

Figure 7: Comparison of $\beta_{opt,a1}$ obtained with three methods (a) Variation of $\beta_{opt,a1}$ with molecular complexity, (b) ξ_{cfd} obtained by simulating $\beta_{opt,a1}$ with the three methods with Toluene as the working fluid.

The fluid-dynamic performance of the vane operating with Toluene at $\beta_{t1} = 6$ calculated with the three methods is plotted against β_{a1} in Figure 7(b). From the outcomes of the analysis, it can be inferred that the use of loss models based on first principles allows one to predict values of post-expansion ratio and total loss in relatively good agreement with those predicted by more computationally expensive CFD-based methods.

5. CONCLUSIONS

The objective of the this work was to investigate the accuracy of an empirical model (Deich et al., 1965) for the prediction of the optimum post-expansion ratio of stator vanes operating with fluids made of complex molecules. To this end, the results obtained by using Deich's model are compared with the optimum post-expansion ratio calculated with a physics-based analytical method and that computed with a high-fidelity CFD-based method.

The methods were applied to stator vanes operating with fluids ranging from a fluid made of simple molecules to a fluid made of complex molecules. The following conclusions can be drawn

1. The optimal performance of axial vanes operating at supersonic flow conditions is characterized by an unique post-expansion ratio which depends on the molecular complexity of the fluid and on the total to static pressure ratio.
2. The empirical method fails to accurately predict the optimum post-expansion ratio for a vane operating at a total to static pressure ratio of 6. Therefore, the empirical method cannot be used to design supersonic vanes of ORC turbines. A new correlation to predict the optimum post-expansion ratio of these vanes is required.
3. The analytical method provides values of the optimal post-expansion ratio well in agreement with those given by the high-fidelity CFD method for the examined fluids and operating conditions.

REFERENCES

Anand, N., Vitale, S., Pini, M., Otero-Rodríguez, G. J., and Pecnik, R. (2018). Design methodology for supersonic radial vanes operating in non-ideal flow conditions. *Journal of Engineering for Gas Turbines and Power*.

Colonna, P., Casati, E., Trapp, C., Mathijssen, T., Larjola, J., Turunen-Saaresti, T., and Uusitalo, A. (2015). Organic rankine cycle power systems: From the concept to current technology, applications, and an outlook to the future. 137:100801–19.

Deich, M. E., Filippov, G. A., and Lazarev, L. Y. (1965). Atlas of Axial Turbine Blade Characteristics. *Mashinostroenie Publishing House*.

Denton, J. D. (1993). Loss mechanisms in turbomachines. *Journal of Turbomachinery*, 115(4):621–656.

Ghidoni, A., Pelizzari, E., Rebay, S., and Selmin, V. (2006). 3d anisotropic unstructured grid generation. *International Journal for Numerical Methods in Fluids*, 51:1097–1115.

Giles, M. B. (1990). Nonreflecting boundary condition for euler equation calculation. *AIAA J.*, 28(12):2050–2058.

Guardone, A., Spinelli, A., and Dossena, V. (2013). Influence of molecular complexity on nozzle design for an organic vapor wind tunnel. *J. Eng. Gas Turb. Power*, 135.

Osnaghi, C. (2013). *Teoria delle Turbomacchine*.

Rinaldi, E., Pecnik, R., and Colonna, P. (2016). Unsteady operation of a highly Supersonic ORC Turbine. *J. Turbomach.*, 138(12).

Vitale, S., Albring, T. A., Pini, M., Gauger, N. R., and Colonna, P. (2017). Fully turbulent discrete adjoint solver for non-ideal compressible flow applications. *Journal of the Global Power and Propulsion Society*, 1.

White, M. and Sayma, A. (2016). Improving the economy-of-scale of small organic Rankine cycle systems through appropriate working fluid selection. *Appl. Energy*, 183:1227–1239.